

Supporting Information

**Bonding state synergy of NiF<sub>2</sub>/Ni<sub>2</sub>P hybrid with co-existence of covalent and ionic bond as a robust catalyst for energy-relevant water and urea electrooxidation**

Hui Liu, Zong Liu and Ligang Feng\*

School of Chemistry and Chemical Engineering, Yangzhou University, Yangzhou 225002, PR  
China.

Email: ligang.feng@yzu.edu.cn; fenglg11@gmail.com (L Feng\*);

## 1. Experimental section

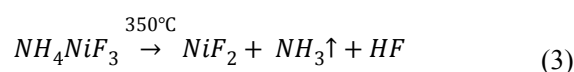
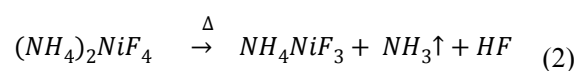
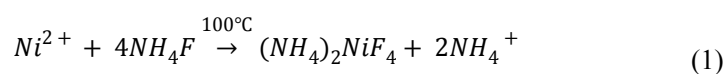
### 1.1 Materials

All chemicals used were of analytical grade and used as received. Nickel nitrate hexahydrate ( $\text{Ni}(\text{NO}_3)_2 \cdot 6\text{H}_2\text{O}$ ), Urea ( $\text{NH}_2\text{CONH}_2$ ), ammonium fluoride ( $\text{NH}_4\text{F}$ ) and Sodium hypophosphite monohydrate ( $\text{NaH}_2\text{PO}_2$ ) are from Aladdin Chemistry Co Ltd. Nafion (5 wt%) is from Sigma-Aldrich Co. Ultrapure water (resistivity  $\geq 18.2 \text{ M}\Omega \text{ cm}^{-1}$ ) was used to prepare the solutions.

### 1.2 Preparation of precursor and $\text{NiF}_2$ , $\text{Ni}_2\text{P}$ , $\text{NiF}_2/\text{Ni}_2\text{P}$

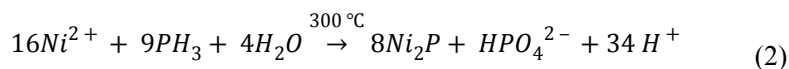
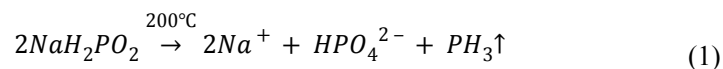
The precursor was synthesized by hydrothermal method.  $\text{Ni}(\text{NO}_3)_2 \cdot 6\text{H}_2\text{O}$ , urea (molar ratio 1:5) and an appropriate amount of ammonium fluoride were added into 30 mL ultrapure water under magnetic stirring to form a homogeneous solution. Then, the obtained solution was transferred into a 50 mL Teflon-lined stainless steel autoclave and heated at 120 °C for 6 h. After cooling down to room temperature, the product was collected by centrifugation and washed with deionized water several times. Finally, it was dried at 60 °C in a vacuum oven for further use.

The as-prepared precursor and ammonium fluoride were loaded into a ceramic boat with a molar ratio of 1:20. The ammonium fluoride was placed at the upstream of the ceramic boat. Then, it was calcined at 350 °C for 2 h under  $\text{N}_2$  protection. After cooling to room temperature,  $\text{NiF}_2$  was achieved by centrifugation and drying in a vacuum oven overnight. The chemical reaction can be express as follows for the  $\text{NiF}_2$  synthesis[1].



The as-prepared precursor and sodium hypophosphite monohydrate were loaded into a ceramic boat with a molar ratio of 1:5 and the sodium hypophosphite monohydrate was placed at the upstream of the ceramic boat. Then, it was calcined at 300 °C for 2 h under  $\text{N}_2$  protection. After cooling to room temperature,  $\text{Ni}_2\text{P}$  was obtained by centrifugation and

drying in a vacuum oven overnight. The relevant chemical reaction can be denoted as below for the Ni<sub>2</sub>P fabrication<sup>[2]</sup>.



Typically, NiF<sub>2</sub> and sodium hypophosphite monohydrate were put into a quartz boat with a molar ratio of 1:5 and calcined at 300 °C for 2 h under N<sub>2</sub> protection in a tube furnace. After cooling to room temperature, NiF<sub>2</sub>/Ni<sub>2</sub>P was obtained by centrifugation and drying in the vacuum oven for use.

### 1.3 Physical characterization

Powder X-ray diffraction (XRD) patterns were tested on a Bruker D8 Advance powder X-ray diffractometer using a Cu K $\alpha$  ( $\lambda = 1.5405 \text{ \AA}$ ) radiation source operating at 40 kV and 40 mA, and at a scanning rate of 5 ° min<sup>-1</sup>. The morphology and microstructure of NiF<sub>2</sub>/Ni<sub>2</sub>P were analyzed by scanning electron microscopy (FESEM, Hitachi, S-4800 II, Japan). All transmission electron microscopy (TEM) and high-resolution TEM (HRTEM) measurements were conducted on a TECNAI G2 operating at 200 kV. The energy dispersive X-ray detector spectrum (EDX) images were obtained on a TECNAI G2 transmission electron microscope equipped with an EDXA detector. All X-Ray photoelectron spectroscopy (XPS) measurements were carried out on a Kratos XSAM-800 spectrometer with an Al K $\alpha$  radiation source. The gas products of NiF<sub>2</sub>/Ni<sub>2</sub>P during oxygen evolution reaction and urea oxidation reaction were probed by gas chromatography (GC, Kechuang, GC9800) equipped with a thermal conductivity detector (TCD), using a packed TDX01 (1m) and molecular sieve 5A column (1.5 m). The carrier gas for TCD is Ar (purity $\geq$ 99.999%), and the detection limit is ca. 50 ppm. The GC calibration curves were generated by running various concentration of the H<sub>2</sub>, O<sub>2</sub>, N<sub>2</sub> using Ar and then response peak area was plotted against the concentration.

### 1.4 Electrochemical measurements

The working electrode is prepared as follows. 4 mg as-prepared catalyst and 1 mg carbon were dispersed entirely into the mixture of 950  $\mu\text{L}$  ethanol and 50  $\mu\text{L}$  Nafion (5 wt %).

After sonicated for 30 min to make a homogeneous solution, 10  $\mu\text{L}$  ink was dropped into the surface of the glass carbon electrode. The electrolyte (1M KOH with and without 0.33 M urea) were saturated by  $\text{N}_2$  atmosphere before use. The catalyst of  $\text{NiF}_2$ ,  $\text{Ni}_2\text{P}$  and  $\text{NiF}_2/\text{Ni}_2\text{P}$  were comparatively studied. The catalyst ink of  $\text{NiF}_2/\text{Ni}_2\text{P}$  without carbon was also prepared with the same approach and studied for relevant electrochemical measurements for comparison.

All the electrochemical measurements were tested in a typical three-electrode system linked to a Bio-Logic SAS analyzer (France). The  $\text{NiF}_2/\text{Ni}_2\text{P}$  electrode was served as the working electrode with a graphite rod as the counter electrode; a saturated calomel electrode (SCE) as the reference electrode was employed through a double salt-bridge and luggin capillary connected to the working electrode and it was calibrated before and after the experiments. The working electrode used was a glassy carbon electrode (3.0 mm diameter). All the potentials used were converted into RHE.  $(E(\text{RHE}) = E(\text{SCE}) + 0.0591 \cdot \text{pH} + 0.24\text{V})$

The catalytic performance of the three samples for OER and UOR were evaluated by cyclic voltammetry (CV) at a scan rate of 5 mV/s. Electrochemical impedance spectroscopy (EIS) which was recorded in the above three-electrode cell with the frequency varies from 1000 kHz to 10 mHz. Chronoamperometry of OER was tested in 1.53V vs RHE and UOR was tested in 1.38V vs RHE. All tests were measured at room temperature (about 25°C).

### **1.5 Overall water splitting and urea electrolysis**

Overall water splitting and urea electrolysis tests were measured in a two-electrode system with the different catalysts as an anode and commercial Pt/C as a cathode. The CV curves were tested in the absence and presence of 0.33M urea in 1M KOH at a scan rate of 5 mV/s with the potential scan range from 1.0 to 1.8 V. The long-term durability of the  $\text{NiF}_2/\text{Ni}_2\text{P}$  electrode was assessed at constant voltage (1.6V) electrolysis. All data for the two electrode tests were recorded without iR correction .

### **1.6 Turnover frequency (TOF) calculation**

The TOF values were calculated from the following equation:

$$TOF = (jA) / (4FQn)$$

$j$  is the current density at overpotential.  $A$  is the surface area of the electrode.  $F$  is the Faraday constant ( $96485 \text{ C mol}^{-1}$ ),  $n$  is the number of moles of active materials that are deposited onto the electrode. The active sites number actually is not easy to obtain, a simple method generally employed by assuming all metal cation as an “active site” was also used here and it was estimated by the number of moles of active materials that are deposited onto the electrode.[3, 4]

$$TOF = \frac{j \times 0.07 \text{ cm}^2 \times 0.001}{4 \times 96485 \times \frac{0.04 \text{ mg} \times 0.001 \times M_{Ni}/M_{total}}{M_{Ni}}}$$

$$TOF_{NiF_2/Ni_2P} = \frac{j_{\eta=350 \text{ mV}} \times 0.07 \text{ cm}^2 \times 0.001}{4 \times 96485 \times \frac{0.04 \text{ mg} \times 0.001 \times 59/119}{59}} = 0.02 \text{ S}^{-1}$$

$$TOF_{Ni_2P} = \frac{j_{\eta=350 \text{ mV}} \times 0.07 \text{ cm}^2 \times 0.001}{4 \times 96485 \times \frac{0.04 \text{ mg} \times 0.001 \times 59/149}{59}} = 0.008 \text{ S}^{-1}$$

$$TOF_{NiF_2} = \frac{j_{\eta=350 \text{ mV}} \times 0.07 \text{ cm}^2 \times 0.001}{4 \times 96485 \times \frac{0.04 \text{ mg} \times 0.001 \times 59/97}{59}} = 0.002 \text{ S}^{-1}$$

$$N_{\text{active sites number}} = n \times N_A$$

$$N_{NiF_2/Ni_2P} = \frac{0.04 \text{ mg} \times 0.001 \times 59/119}{59} \times N_A = 2.02 \times 10^{17}$$

$$N_{NiF_2} = \frac{0.04 \text{ mg} \times 0.001 \times 59/97}{59} \times N_A = 2.48 \times 10^{17}$$

$$N_{Ni_2P} = \frac{0.04 \text{ mg} \times 0.001 \times 59/149}{59} \times N_A = 1.62 \times 10^{17}$$

### 1.7 Faradaic efficiency calculation for OER

A gas-tight electrochemical cell coupling with a gas sensor to evaluate the gas produced was used to probe the faradaic yield of  $NiF_2/Ni_2P$ . The working electrode was prepared by drop-casting catalyst suspension on the glassy carbon electrode with the surface area of  $0.07 \text{ cm}^2$ . A constant potential ( $1.53 \text{ V vs. RHE}$ ) was applied on the electrode and the volume of the

evolved gas was recorded synchronously. Thus, the faradaic yield was calculated from the ratio of the recorded gas volume to the theoretical gas volume during the charge passed through the electrode[5].

$$\text{Faradaic yield} = \frac{V_{\text{experimental}}}{V_{\text{theoretical}}} = \frac{V_{\text{experimental}}}{\frac{1}{4} \times \frac{Q}{F} \times V_m}$$

where Q is the charge passed through the electrode, F is Faraday constant (96485 C mol<sup>-1</sup>), the number 4 means 4 mole electrons per mole O<sub>2</sub>, V<sub>m</sub> is the molar volume of gas (24.5 L mol<sup>-1</sup>, 298 K, 101 KPa).

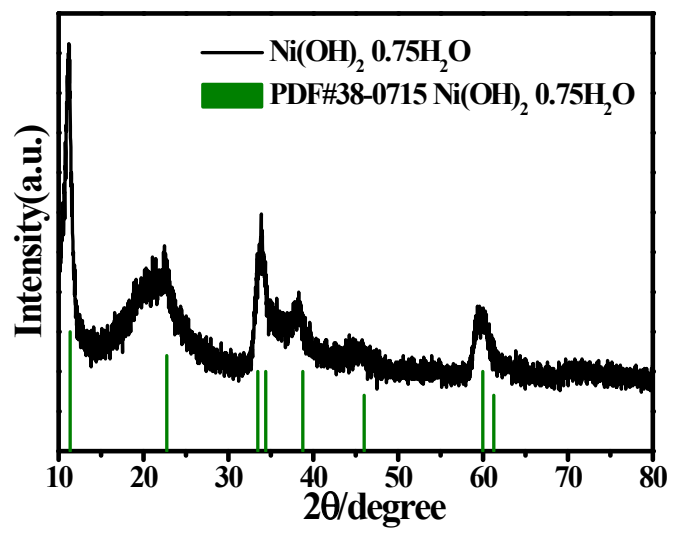
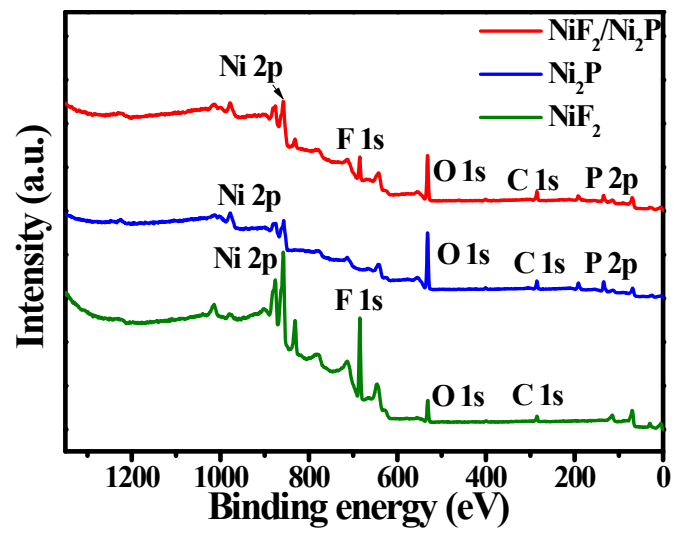
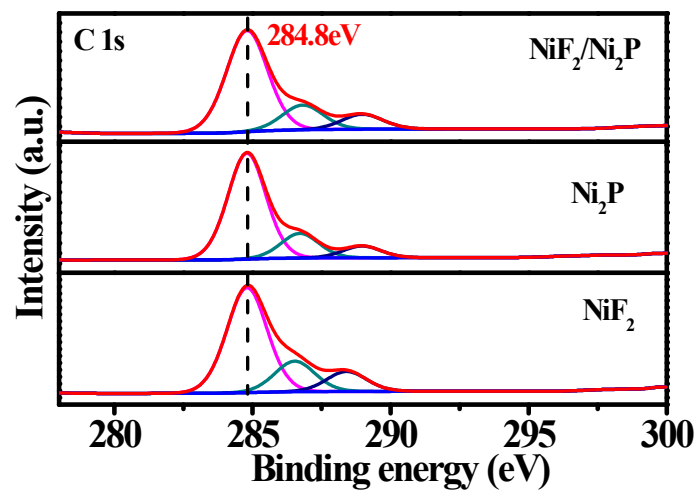


Figure S1a. XRD pattern of the precursor.



**Figure S1b.** XPS survey spectra for NiF<sub>2</sub>, Ni<sub>2</sub>P and NiF<sub>2</sub>/Ni<sub>2</sub>P.



**Figure S2.** XPS spectra of C 1s for NiF<sub>2</sub>, Ni<sub>2</sub>P and NiF<sub>2</sub>/Ni<sub>2</sub>P.

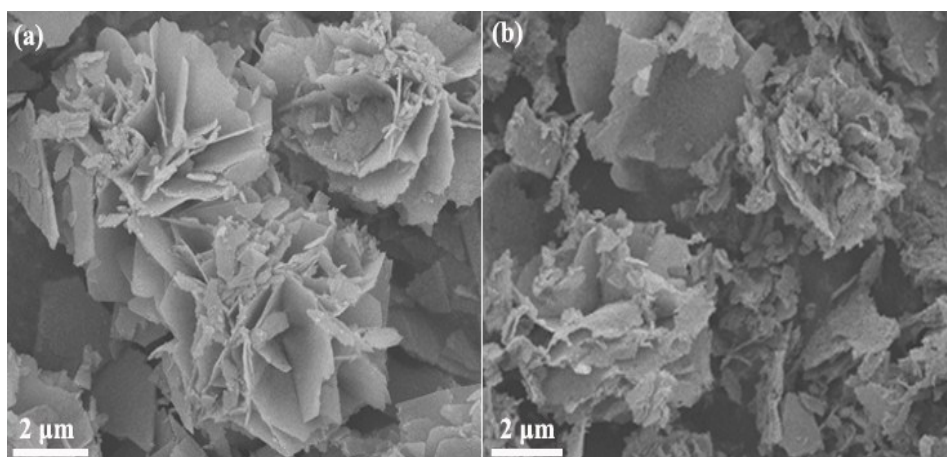


**Figure S3a.** SEM images of NiF<sub>2</sub> (a) and Ni<sub>2</sub>P catalysts (b).

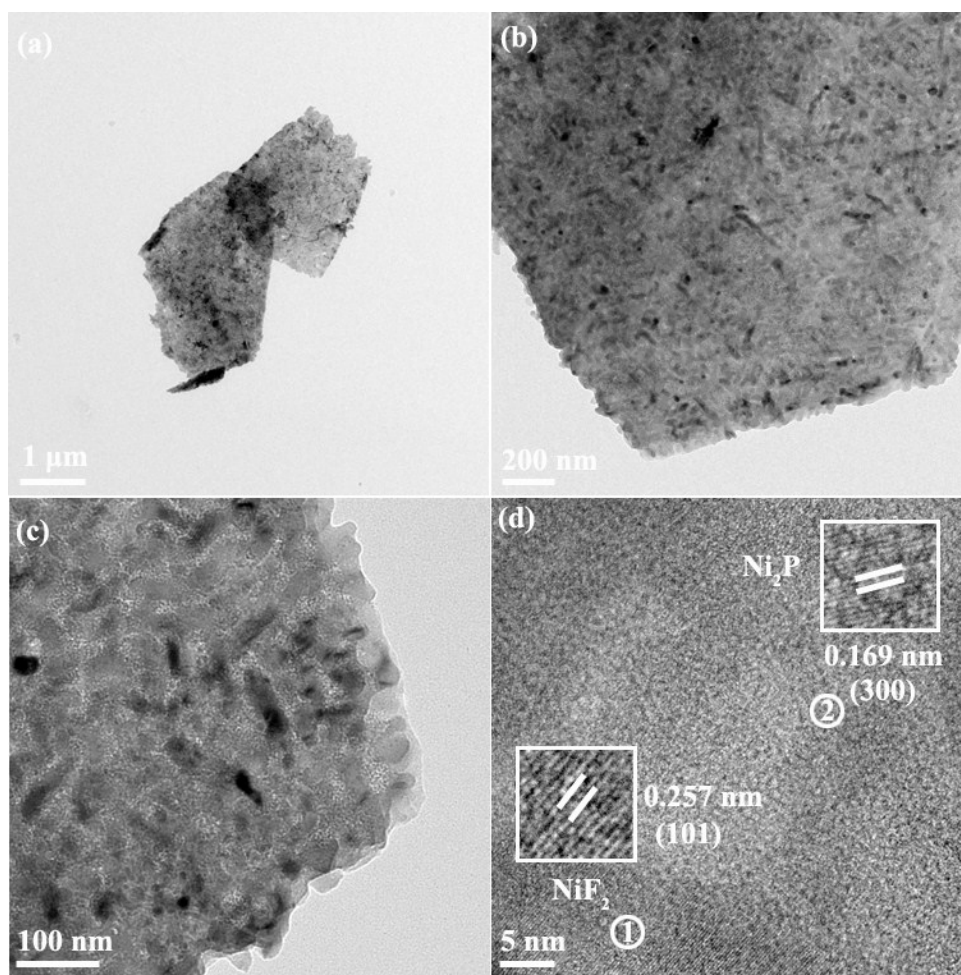


**Figure S3b.** TEM images (a-c) and HRTEM image of NiF<sub>2</sub>/Ni<sub>2</sub>P (d).

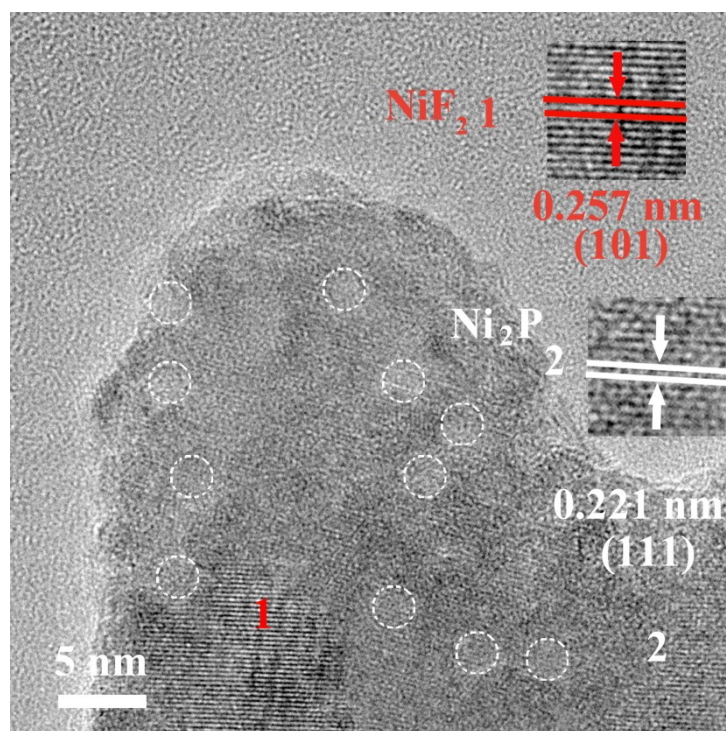


**Figure S3c.** HRTEM image of  $\text{NiF}_2/\text{Ni}_2\text{P}$ .

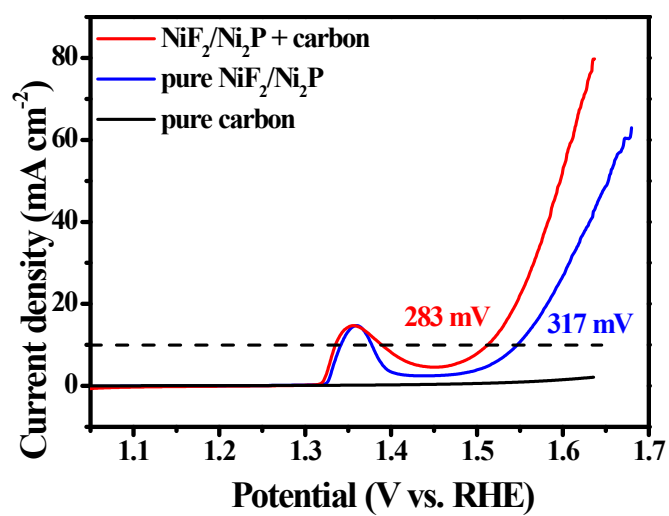


**Figure S4a.** Polarization curves of NiF<sub>2</sub>/Ni<sub>2</sub>P with and without carbon and pure carbon in 1 M KOH electrolyte at 5 mV/s.

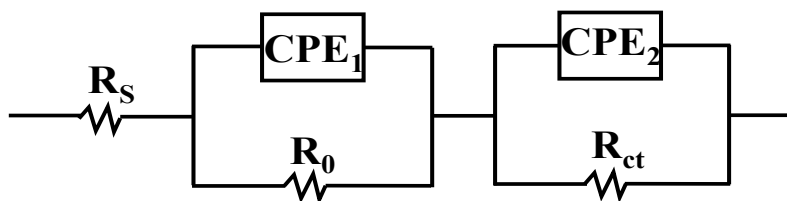


**Figure S4b.** Equivalent circuit diagram for fitting the EIS data.

$R_s$  means uncompensated solution resistance,  $R_{ct}$  is a charge transfer resistance,  $R_o$  is associated to the contact resistance between the catalysts and The CPE generally was employed to well fit the impedance data by safely treating as an empirical constant without considering the its physical basis. And mostly, it was regarded as the double layer capacitor from the catalyst/support and catalyst solution.

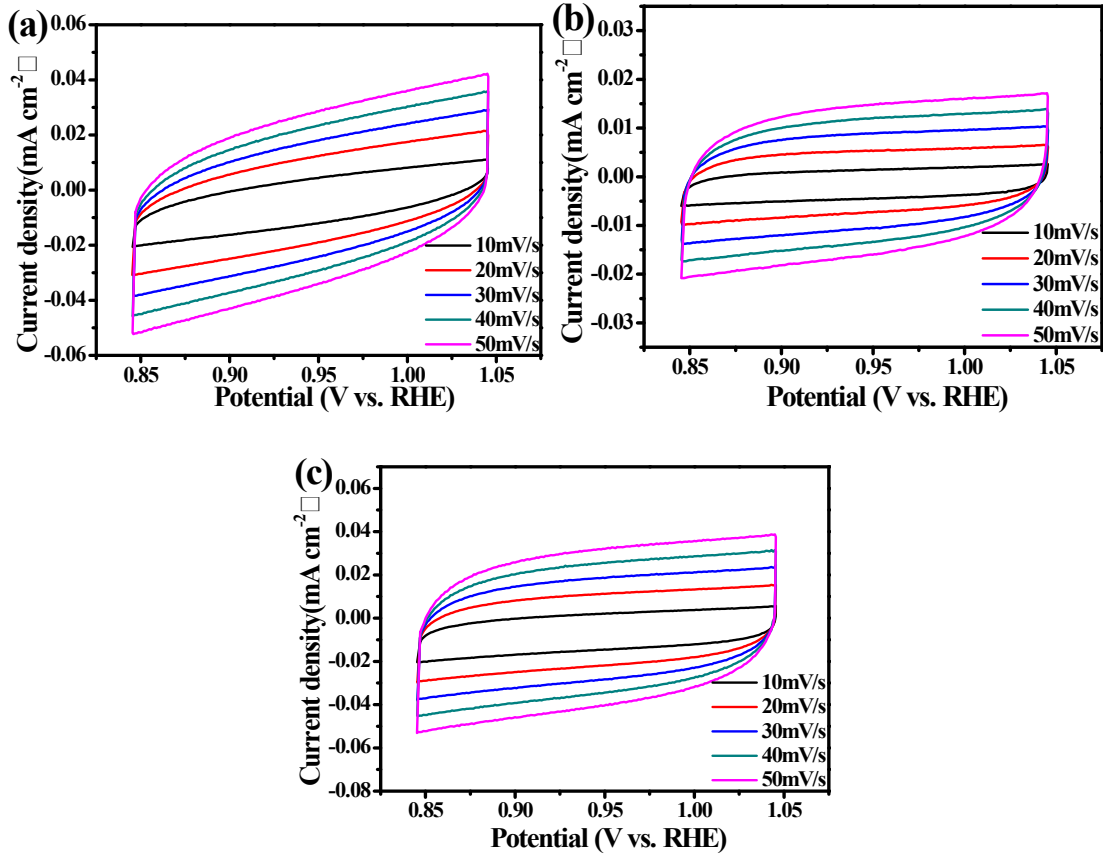


Figure S5. Cyclic voltammetry (CV) curves of NiF<sub>2</sub> (a), Ni<sub>2</sub>P (b) and NiF<sub>2</sub>/Ni<sub>2</sub>P (c) with various scan rates (10–50 mV/s) in the 0.83 to 1.03 V vs RHE region.

The ECSA was calculated by measuring the capacitive current associated with double-layer charging from the cyclic voltammetry (CV) curves at different scan rates. A linear slope is obtained from the plot of the differences in the charging current density ( $J_a - J_c$ ) at 0.93 V (vs. RHE) against the scan rate.

Calculation of electrochemical active surface area (ECSA):

$$ECSA = \frac{C_{dl}}{C_s}$$

where the specific capacitance value was 40  $\mu\text{F cm}^{-2}$  [6].

$$ECSA_{NiF_2} = \frac{0.568 \text{ mF cm}^{-2} \times 0.07 \text{ cm}^2}{0.04 \text{ mF cm}^{-2}} = 0.994 \text{ cm}^2$$

$$ECSA_{Ni_2P} = \frac{0.311 \text{ mF cm}^{-2} \times 0.07 \text{ cm}^2}{0.04 \text{ mF cm}^{-2}} = 0.544 \text{ cm}^2$$

$$ECSA_{NiF2/Ni2P} = \frac{0.692 \text{ mF cm}^{-2} \times 0.07 \text{ cm}^2}{0.04 \text{ mF cm}^{-2}} = 1.211 \text{ cm}^2$$

Roughness Factor (RF) [7]:

$$\text{Roughness Factor (RF)} = \frac{\text{Electrochemical surface area (ECSA)}}{\text{Geometrical surface area (GSA)}}$$

$$RF_{NiF2} = \frac{0.994 \text{ cm}^2}{0.07 \text{ cm}^2} = 14.2$$

$$RF_{Ni2P} = \frac{0.544 \text{ cm}^2}{0.07 \text{ cm}^2} = 7.77$$

$$RF_{NiF2/Ni2P} = \frac{1.211 \text{ cm}^2}{0.07 \text{ cm}^2} = 17.3$$

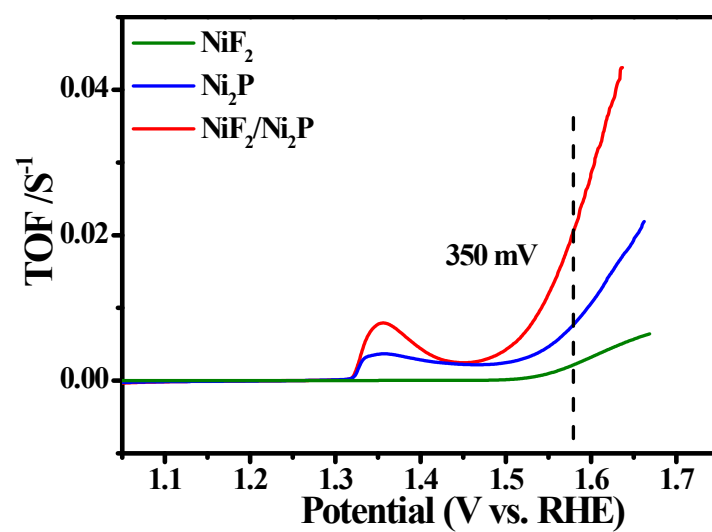


**Figure S6.** The turnover frequency curve for NiF<sub>2</sub>, Ni<sub>2</sub>P and NiF<sub>2</sub>/Ni<sub>2</sub>P.

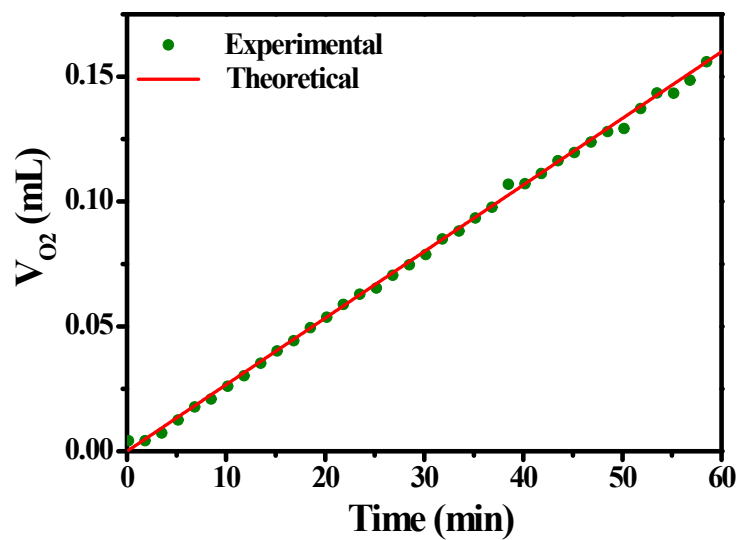


**Figure S7.** Faradaic efficiency of NiF<sub>2</sub>/Ni<sub>2</sub>P. The amount of O<sub>2</sub> produced during the electrolysis matches well with the theoretic amount of O<sub>2</sub> generated assuming four electrons transferred for one oxygen indicating a nearly 100% current efficiency.

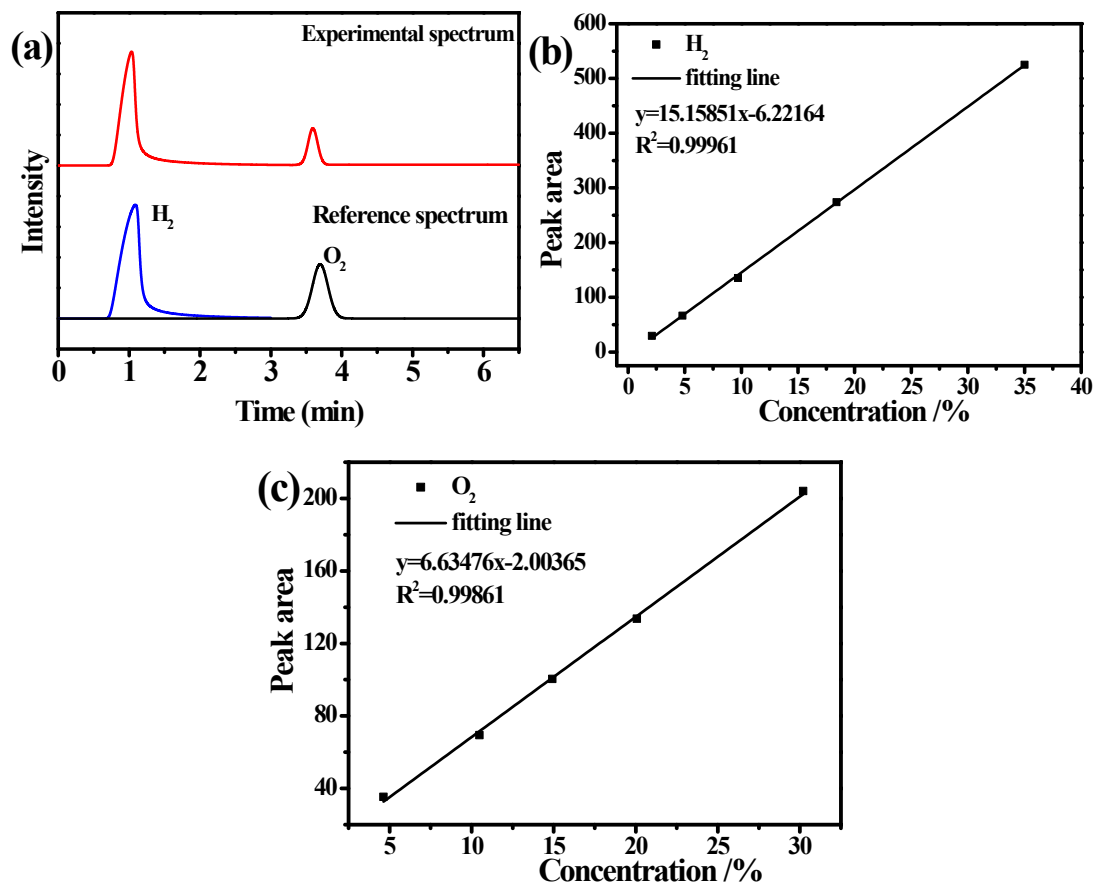


**Figure S8.** Purity of the gas obtained from water splitting measured by gas chromatography spectrum (a). Calibration curves for H<sub>2</sub> (b) and O<sub>2</sub> (c).

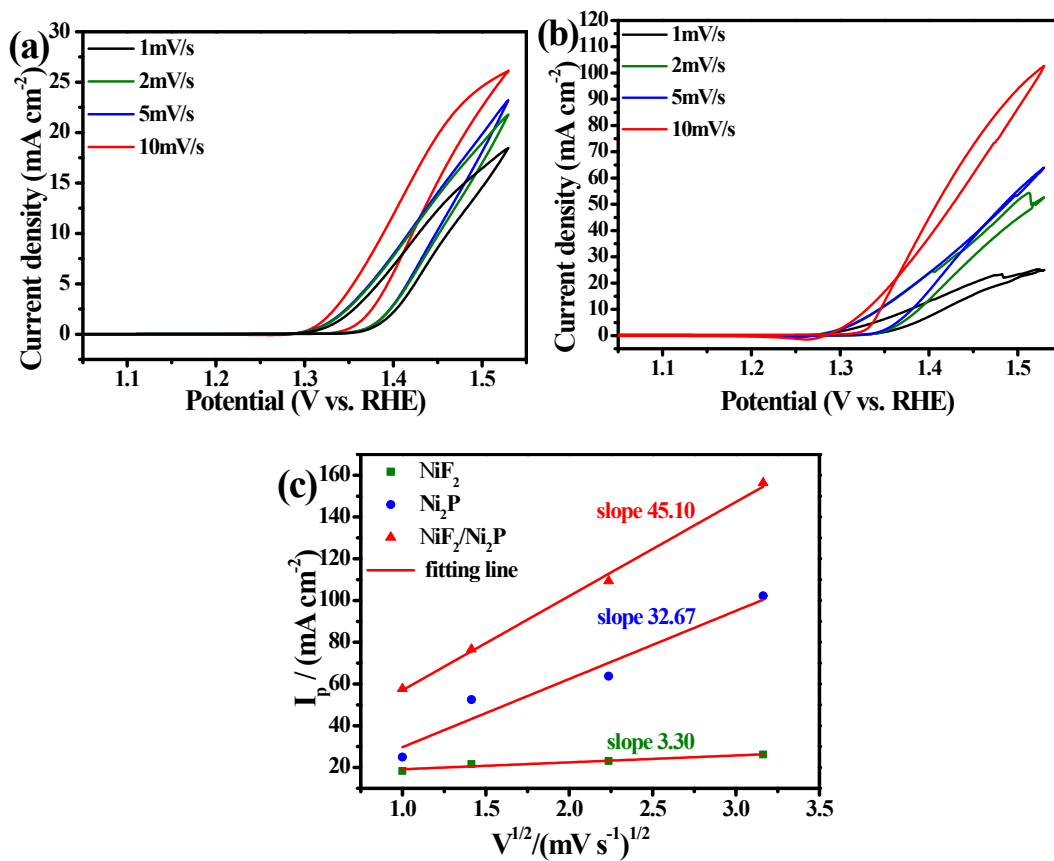


**Figure S9.** CV curves of  $\text{NiF}_2$  (a) and  $\text{Ni}_2\text{P}$  (b) in 1.0 M KOH with 0.33M urea at different scan rates from 1 to 10 mV/s. Variation of urea oxidation peak current density values at different catalysts with the square root of scan rate. (c)

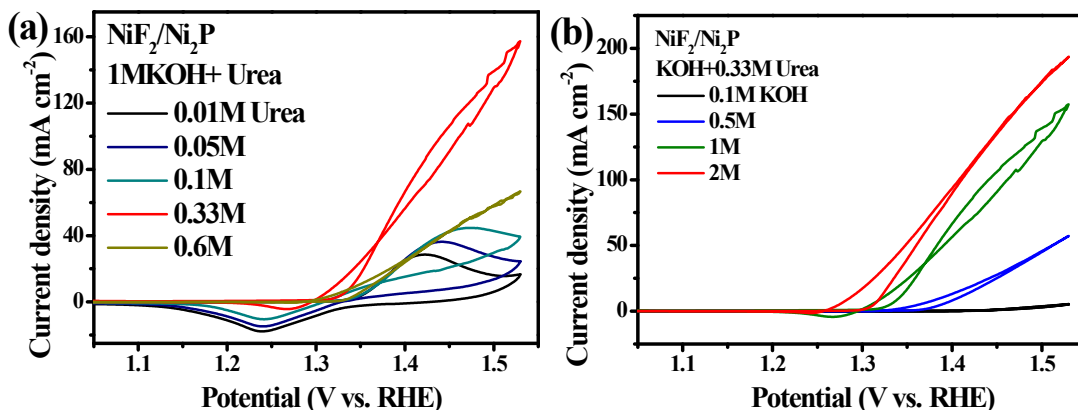


**Figure S10.** Effect of urea concentrations on the electrocatalytic oxidation of urea at  $\text{NiF}_2/\text{Ni}_2\text{P}$  electrode in 1M KOH at a scan rate of 10 mV/s, the concentration of urea used was (1) 0.01 M, (2) 0.05 M, (3) 0.1 M, (4) 0.33 M, (5) 0.66M.(a) Effect of KOH concentrations on the electrocatalytic oxidation of urea at  $\text{NiF}_2/\text{Ni}_2\text{P}$  electrode in 0.33 M urea at a scan rate of 10 mV/s, the concentration of KOH used was (1) 0.1 M, (2) 0.5 M, (3) 1 M, (4) 2 M.(b)

The reaction kinetics for urea oxidation was relevant to the concentration of urea and  $\text{OH}^-$ . The effect of urea concentration from 0.01 to 0.66 M in 1M KOH electrolyte was investigated for urea oxidation. As can be seen, increasing the concentration of urea gave rise to larger activity until concentrations of 0.33 M. The activity was not improved further by increasing the concentration from 0.33 to 0.66 M. The urea oxidation peak was clearly observed due to the insufficient urea (from 0.01 to 0.1 M) available for the reaction, thus a broad oxidation peak was found in the forward scan direction and no such high oxidation current was found in the backward scan direction. Sufficient urea was available for the active sites by increasing urea concentration to 0.33M, a similar oxidation current was obtained for the forward and backward scan direction. When the urea concentration reached 0.66 M, the local surface coverage of the Ni catalyst by excess urea and reaction products will restrict the contact with  $\text{OH}^-$  as the  $\text{OH}^-$  is required for the formation of  $\text{NiOOH}$ , the active catalyst for UOR. Thus the performance was reduced. Similar case was found on the effect of KOH concentrations. The performance of urea oxidation was increased by increasing the KOH concentration and it can be attributed to the increased ion conductivity and  $\text{NiOOH}$  active sites for the reaction. By increasing the KOH concentration, more active sites of  $\text{NiOOH}$  can be formed, the improved catalytic performance like higher oxidation current and reduced onset potential was found.[8, 9]

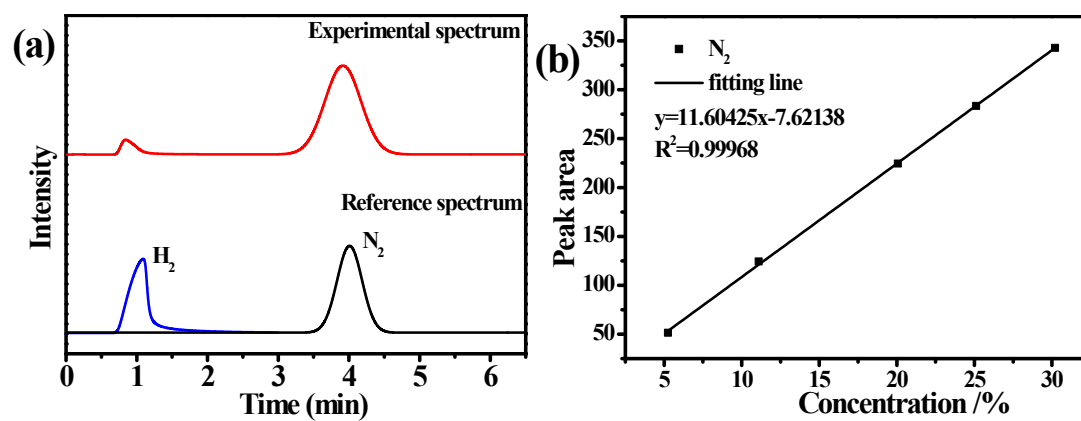


**Figure S11a.** Purity of gas obtained from urea oxidation measured by gas chromatography spectrum  
(a). Calibration curve for N<sub>2</sub> (b).

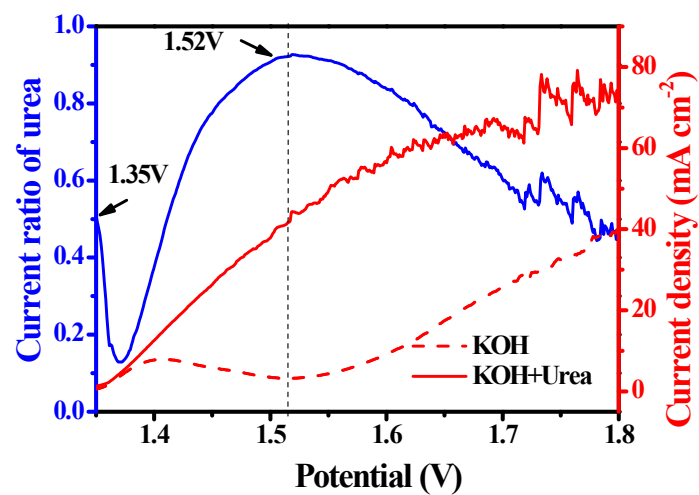


**Figure S11b.** Current contribution from urea in the two-electrode water splitting system of Pt/C||NiF<sub>2</sub>/Ni<sub>2</sub>P electrode in 1M KOH with 0.33 M urea, it was plotted by (1-current obtained from KOH/ current obtained in 1M KOH with 0.33 M urea).

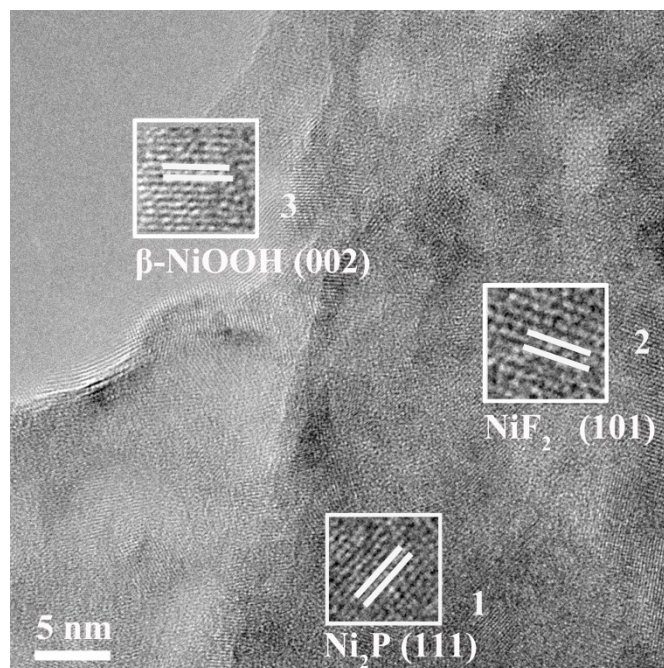


**Figure S11c.** HRTEM image of  $\text{NiF}_2/\text{Ni}_2\text{P}$  after stability test.

Table S1. The binding energy of Ni 2p components for all samples.

Catalysts	Binding energy/eV					
	Ni 2p <sub>1/2</sub>		Ni 2p <sub>3/2</sub>			
		satellite		satellite		
NiF <sub>2</sub>	875.6	863.4	857.6	881.3		
Ni <sub>2</sub> P	870.1	874.7	862.5	852.9	856.7	880.8
NiF <sub>2</sub> /Ni <sub>2</sub> P	870.1	875.6	863.2	852.9	857.6	881.3

Table S2. OER performance comparison of NiF<sub>2</sub>/Ni<sub>2</sub>P and some Ni-Based electrocatalysts.

Catalysts	electrolytes	Electrode substrate	Overpotential	Reference
			at 10 mA cm <sup>-2</sup> (mV)	
NiF <sub>2</sub> /Ni <sub>2</sub> P	1 M KOH	glassy carbon	283	This work
Ni(OH) <sub>2</sub>	1 M KOH	glassy carbon	299	[10]
NiCo <sub>2</sub> O <sub>4</sub>	0.1 M KOH	glassy carbon	340	[11]
NiS	1 M KOH	glassy carbon	320	[12]
Ni <sub>3</sub> N/NC	1.0 M KOH	glassy carbon	310	[13]
Ni <sub>3</sub> Te <sub>2</sub>	1 M KOH	glassy carbon	315	[14]
Ni <sub>3</sub> Se <sub>2</sub>	0.3 M KOH	glassy carbon	290	[15]
Co-Ni-B	1 M KOH	glassy carbon	330	[16]
Ni <sub>2</sub> P	1.0 M KOH	glassy carbon	359	[17]
Au/Ni <sub>12</sub> P <sub>5</sub>	1.0 M KOH	glassy carbon	340	[18]
Ni@Pt	1 M KOH	glassy carbon	290	[19]
NiO/CNT	1.0 M KOH	glassy carbon	315	[20]
Se-NiMn LDH	1.0 M KOH	glassy carbon	280	[21]
NiFe LDH/C	0.1 M KOH	glassy carbon	360	[22]
NiFe LDH-NO <sub>3</sub> <sup>-</sup>	0.1 M KOH	glassy carbon	275	[23]
NiFe LDH	1.0 M KOH	glassy carbon	300	[24]
Ni <sub>32</sub> Fe oxide	1 M KOH	glassy carbon	370	[25]
NiFe <sub>2</sub> O <sub>4</sub>	0.1 M KOH	glassy carbon	440	[26]
NiCo <sub>2</sub> O <sub>4</sub> /NiO	1 M NaOH	glassy carbon	360	[27]
NiFe LDH-MoO <sub>4</sub> <sup>2-</sup>	1 M KOH	glassy carbon	280	[28]
NiFe@C	1 M KOH	glassy carbon	281	[29]
NiFe/C	0.1 M KOH	glassy carbon	240	[30]
Ni-Fe oxide	0.1 M KOH	glassy carbon	328	[31]
Ni <sub>0.62</sub> Fe <sub>0.38</sub> P	1 M KOH	glassy carbon	290	[32]

---

NiCoFeP	1 M KOH	glassy carbon	273	[33]
Ni <sub>2</sub> CoS <sub>4</sub>	1 M KOH	glassy carbon	290	[34]
Ni-Co sulfide	1 M KOH	glassy carbon	322	[35]
NiFeB	1 M KOH	glassy carbon	251	[36]

---

Table S3. EIS fitting parameters form equivalent circuits for all samples in 1M KOH.

Catalysts	$R_s/\Omega$	$CPE/S\ s^{-n}$	$CPE/S\ s^{-n}$	$n/0 < n < 1$	$R_{ct}/\Omega$	$R_o/\Omega$
NiF <sub>2</sub>	9.25	1.009E-004	1.152E-003	0.97	6.117E+002	1.620E+002
Ni <sub>2</sub> P	8.24	6.950E-006	2.179E-005	0.80	3.920E+002	5.790E+001
NiF <sub>2</sub> /Ni <sub>2</sub> P	8.95	5.306E-006	7.748E-003	0.66	6.200E+001	9.477E+000

Table S4. Urea oxidation performance comparison of NiF<sub>2</sub>/Ni<sub>2</sub>P and some Ni-based materials.

Catalysts	Electrolytes	Onset potential ( vs RHE)	Current density at 1.5V (mA cm <sup>-2</sup> )	Reference
NiF <sub>2</sub>	1M KOH+0.33M Urea	1.37 V	20	this work
Ni <sub>2</sub> P	1M KOH+0.33M Urea	1.33 V	86	this work
NiF <sub>2</sub> /Ni <sub>2</sub> P	1M KOH+0.33M Urea	1.31V	128	this work
NF@NiO	1M KOH+0.33M Urea	1.33V	70	[37]
Ni-P	1M KOH+0.33M Urea	1.37V	60	[38]
Ni(OH) <sub>2</sub> /C	1M KOH+0.33M Urea	1.35V	40	[39]
Ni/C	1M KOH+0.33M Urea	1.33V	30	[40]
β Ni(OH) <sub>2</sub>	1M KOH+0.33M Urea	1.37V	2	[41]
Ni-WC/MWCNT	1M KOH+0.33M Urea	1.38V	10	[42]
Ni/Sn-dendrites	1M KOH+0.33M Urea	1.33V	30	[43]
Ni-MOF	1M KOH+0.33M Urea	1.35V	75	[44]
NiO/Gr-200	0.5MNaOH+0.3M Urea	1.42V	15	[45]

Table S5. EIS fitting parameters form equivalent circuits for all samples in 1M KOH and 0.33M urea.

Catalysts	$R_s/\Omega$	CPE/S $s^{-n}$	CPE/S $s^{-n}$	$n/0 < n < 1$	$R_{ct}/\Omega$	$R_o/\Omega$
NiF <sub>2</sub>	8.71	9.265E-005	3.385E-002	0.86	1.940E+003	1.000E+001
Ni <sub>2</sub> P	6.95	5.103E-005	1.043E-004	0.88	1.542E+003	1.900E+001
NiF <sub>2</sub> /Ni <sub>2</sub> P	7.21	6.712E-005	2.604E-004	0.89	1.092E+003	2.364E+000

Table S6. Comparison of current density for three catalysts at 1.6 V vs RHE in 1M KOH with and without 0.33M Urea.

Catalysts	Electrolyte	Current density(mA cm <sup>-2</sup> )
NiF <sub>2</sub>		0.42
Ni <sub>2</sub> P	KOH	3.90
NiF <sub>2</sub> /Ni <sub>2</sub> P		10.2
NiF <sub>2</sub>		1.66
Ni <sub>2</sub> P	KOH + Urea	24.1
NiF <sub>2</sub> /Ni <sub>2</sub> P		56.8

Table S7. Elemental composition of NiF<sub>2</sub>/Ni<sub>2</sub>P after durability test analyzed by XPS.

NiF <sub>2</sub> /Ni <sub>2</sub> P	Atomic composition (%)			
	element	Ni	F	P
Before test	19.73	16.07	15.14	49.06
After test	11.96	NA	NA	88.04

## References

- [1] J. Chun, C. Jo, S. Sahgong, M.G. Kim, E. Lim, D.H. Kim, J. Hwang, E. Kang, K.A. Ryu, Y.S. Jung, Y. Kim, J. Lee, Ammonium Fluoride Mediated Synthesis of Anhydrous Metal Fluoride–Mesoporous Carbon Nanocomposites for High-Performance Lithium Ion Battery Cathodes, *ACS Appl Mater Interfaces*, **2016**, *8*, 35180-35190.
- [2] R. Prins, M.E. Bussell, Metal Phosphides: Preparation, Characterization and Catalytic Reactivity, *Catal Lett*, **2012**, *142*, 1413-1436.
- [3] T. Zhou, Z. Cao, P. Zhang, H. Ma, Z. Gao, H. Wang, Y. Lu, J. He, Y. Zhao, Transition metal ions regulated oxygen evolution reaction performance of Ni-based hydroxides hierarchical nanoarrays, *Sci. Rep.*, **2017**, *7*, 46154.
- [4] M. Gao, W. Sheng, Z. Zhuang, Q. Fang, S. Gu, J. Jiang, Y. Yan, Efficient Water Oxidation Using Nanostructured  $\alpha$ -Nickel-Hydroxide as an Electrocatalyst, *J Am Chem Soc*, **2014**, *136*, 7077-7084.
- [5] J. Wang, K. Li, H.-x. Zhong, D. Xu, Z.-l. Wang, Z. Jiang, Z.-j. Wu, X.-b. Zhang, Synergistic effect between metal-nitrogen-carbon sheets and NiO nanoparticles for enhanced electrochemical water-oxidation performance, *Angew. Chem. Int. Ed.*, **2015**, *54*, 10530-10534.
- [6] B. Zhao, R. Ran, L. Sun, Z. Yang, X. Wu, D. Weng, A high-surface-area La-Ce-Mn mixed oxide with enhanced activity for CO and C<sub>3</sub>H<sub>8</sub> oxidation, *Catal. Commun.*, **2018**, *105*, 26-30.
- [7] C.C.L. McCrory, S. Jung, J.C. Peters, T.F. Jaramillo, Benchmarking Heterogeneous Electrocatalysts for the Oxygen Evolution Reaction, *J. Am. Chem. Soc.*, **2013**, *135*, 16977-16987.
- [8] R.P. Forslund, J.T. Mefford, W.G. Hardin, C.T. Alexander, K.P. Johnston, K.J. Stevenson, Nanostructured LaNiO<sub>3</sub> Perovskite Electrocatalyst for Enhanced Urea Oxidation, *ACS Catal.*, **2016**, *6*, 5044-5051.
- [9] R.M. Tesfaye, G. Das, B.J. Park, J. Kim, H.H. Yoon, Ni-Co bimetal decorated carbon nanotube aerogel as an efficient anode catalyst in urea fuel cells, *Sci. Rep.*, **2019**, *9*, 479.
- [10] L.-A. Stern, X. Hu, Enhanced oxygen evolution activity by NiO<sub>x</sub> and Ni(OH)<sub>2</sub> nanoparticles, *Faraday Discuss*, **2014**, *176*, 363-379.
- [11] X. Lv, Y. Zhu, H. Jiang, X. Yang, Y. Liu, Y. Su, J. Huang, Y. Yao, C. Li, Hollow mesoporous NiCo<sub>2</sub>O<sub>4</sub> nanocages as efficient electrocatalysts for oxygen evolution reaction, *Dalton Trans.*, **2015**, *44*, 4148-4154.
- [12] P. Luo, H. Zhang, L. Liu, Y. Zhang, J. Deng, C. Xu, N. Hu, Y. Wang, Targeted synthesis of unique Nickel sulfide (NiS, NiS<sub>2</sub>) microarchitectures and the applications for the enhanced water splitting system, *ACS Appl. Mater. Interfaces*, **2017**, *9*, 2500-2508.
- [13] M. Chen, J. Qi, D. Guo, H. Lei, W. Zhang, R. Cao, Facile synthesis of sponge-like Ni<sub>3</sub>N/NC for electrocatalytic water oxidation, *Chem. Commun.*, **2017**, *53*, 9566-9569.
- [14] Z. Wang, L. Zhang, Nickel Ditelluride Nanosheet Arrays: A Highly Efficient Electrocatalyst for the Oxygen Evolution Reaction, *ChemElectroChem*, **2018**, *5*, 1153-1158.
- [15] A.T. Swesi, J. Masud, M. Nath, Nickel selenide as a high-efficiency catalyst for oxygen evolution reaction, *Energy Environ. Sci.*, **2016**, *9*, 1771-1782.
- [16] J. Zhang, X. Li, Y. Liu, Z. Zeng, X. Cheng, Y. Wang, W. Tu, M. Pan, Bi-metallic boride electrocatalysts with enhanced activity for the oxygen evolution reaction, *Nanoscale*, **2018**, *10*, 11997-12002.
- [17] H. Sun, X. Xu, Z. Yan, X. Chen, F. Cheng, P.S. Weiss, J. Chen, Porous multishelled Ni<sub>2</sub>P hollow microspheres as an active electrocatalyst for hydrogen and oxygen evolution, *Chem. Mater.*, **2017**, *29*, 8539-8547.
- [18] Y. Xu, S. Duan, H. Li, M. Yang, S. Wang, X. Wang, R. Wang, Au/Ni<sub>12</sub>P<sub>5</sub> core/shell single-crystal nanoparticles as oxygen evolution reaction catalyst, *Nano Research*, **2017**, *10*, 3103-3112.
- [19] F. Wang, G. Chen, X. Liu, F. Chen, H. Wan, L. Ni, N. Zhang, R. Ma, G. Qiu, Advanced Electrocatalytic Performance of Ni-Based Materials for Oxygen Evolution Reaction, *Acs Sustain Chem Eng*, **2019**, *7*, 341-349.
- [20] Y. Fan, Y. Wu, G. Clavel, M.H. Raza, P. Amsalem, N. Koch, N. Pinna, Optimization of the Activity of Ni-Based Nanostructures for the Oxygen Evolution Reaction, *ACS Appl. Energy Mater.*, **2018**, *1*, 4554-4563.

- [21] J. Du, Z. Zou, A. Yu, C. Xu, Selenization of NiMn-layered double hydroxide with enhanced electrocatalytic activity for oxygen evolution, *Dalton Trans.*, **2018**, 47, 7492-7497.
- [22] F. Dionigi, T. Reier, Z. Pawolek, M. Glicch, P. Strasser, Design Criteria, Operating Conditions, and Nickel–Iron Hydroxide Catalyst Materials for Selective Seawater Electrolysis, *ChemSusChem*, **2016**, 9, 962-972.
- [23] Y. Xu, Y. Hao, G. Zhang, Z. Lu, S. Han, Y. Li, X. Sun, Room-temperature synthetic NiFe layered double hydroxide with different anions intercalation as an excellent oxygen evolution catalyst, *RSC Adv*, **2015**, 5, 55131-55135.
- [24] F. Song, X. Hu, Exfoliation of layered double hydroxides for enhanced oxygen evolution catalysis, *Nat Commun*, **2014**, 5, 4477.
- [25] M. Yu, G. Moon, E. Bill, H. Tueysuez, Optimizing Ni-Fe Oxide Electrocatalysts for Oxygen Evolution Reaction by Using Hard Templating as a Toolbox, *ACS Appl. Energy Mater.*, **2019**, 2, 1199-1209.
- [26] M. Li, W. Wang, M. Yang, F. Lv, L. Cao, Y. Tang, R. Sun, Z. Lu, Large-scale fabrication of porous carbon-decorated iron oxide microcuboids from Fe-MOF as high-performance anode materials for lithium-ion batteries, *Rsc Adv.*, **2015**, 5, 7356-7362.
- [27] C. Mahala, M. Basu, Nanosheets of NiCo<sub>2</sub>O<sub>4</sub>/NiO as Efficient and Stable Electrocatalyst for Oxygen Evolution Reaction, *ACS Omega*, **2017**, 2, 7559-7567.
- [28] N. Han, F. Zhao, Y. Li, Ultrathin nickel–iron layered double hydroxide nanosheets intercalated with molybdate anions for electrocatalytic water oxidation, *J Mater Chem A*, **2015**, 3, 16348-16353.
- [29] Y. Feng, X.-Y. Yu, U. Paik, N-doped graphene layers encapsulated NiFe alloy nanoparticles derived from MOFs with superior electrochemical performance for oxygen evolution reaction, *Sci. Rep.*, **2016**, 6, 34004.
- [30] Y. Feng, H. Zhang, Y. Zhang, X. Li, Y. Wang, Ultrathin Two-Dimensional Free-Standing Sandwiched NiFe/C for High-Efficiency Oxygen Evolution Reaction, *ACS Appl Mater Interfaces*, **2015**, 7, 9203-9210.
- [31] J. Qi, W. Zhang, R. Xiang, K. Liu, H.-Y. Wang, M. Chen, Y. Han, R. Cao, Porous Nickel–Iron Oxide as a Highly Efficient Electrocatalyst for Oxygen Evolution Reaction, *Adv. Sci.*, **2015**, 2, 1500199.
- [32] H.-H. Zou, C.-Z. Yuan, H.-Y. Zou, T.-Y. Cheang, S.-J. Zhao, U.Y. Qazi, S.-L. Zhong, L. Wang, A.-W. Xu, Bimetallic phosphide hollow nanocubes derived from a prussian-blue-analog used as high-performance catalysts for the oxygen evolution reaction, *Catal. Sci. Technol.*, **2017**, 7, 1549-1555.
- [33] Y. Guo, J. Tang, Z. Wang, Y. Sugahara, Y. Yamauchi, Hollow Porous Heterometallic Phosphide Nanocubes for Enhanced Electrochemical Water Splitting, *Small*, **2018**, 14, 1802442.
- [34] Y.-R. Hong, S. Mhin, K.-M. Kim, W.-S. Han, H. Choi, G. Ali, K.Y. Chung, H.J. Lee, S.-I. Moon, S. Dutta, S. Sun, Y.-G. Jung, T. Song, H. Han, Electrochemically activated cobalt nickel sulfide for an efficient oxygen evolution reaction: partial amorphization and phase control, *J Mater Chem A*, **2019**, 7, 3592-3602.
- [35] Y.-R. Hong, S. Mhin, J. Kwon, W.-S. Han, T. Song, H. Han, Synthesis of transition metal sulfide and reduced graphene oxide hybrids as efficient electrocatalysts for oxygen evolution reactions, *R. Soc. Open Sci.*, **2018**, 5, 180927.
- [36] G. Liu, D. He, R. Yao, Y. Zhao, J. Li, Amorphous NiFeB nanoparticles realizing highly active and stable oxygen evolving reaction for water splitting, *Nano Res.*, **2018**, 11, 1664-1675.
- [37] M.-S. Wu, F.-Y. Chen, Y.-H. Lai, Y.-J. Sie, Electrocatalytic oxidation of urea in alkaline solution using nickel/nickel oxide nanoparticles derived from nickel-organic framework, *Electrochim Acta*, **2017**, 258, 167-174.
- [38] R. Ding, X. Li, W. Shi, Q. Xu, L. Wang, H. Jiang, Z. Yang, E. Liu, Mesoporous Ni-P nanocatalysts for alkaline urea electrooxidation, *Electrochim Acta*, **2016**, 222, 455-462.
- [39] D. Wang, S. Liu, Q. Gan, J. Tian, T.T. Isimjan, X. Yang, Two-dimensional nickel hydroxide nanosheets with high-content of nickel (III) species towards superior urea electro-oxidation, *J. Electroanal. Chem.*, **2018**, 829, 81-87.
- [40] L. Wang, L.T. Ren, X.R. Wang, X. Feng, J.W. Zhou, B. Wang, Multivariate MOF-Templated Pomegranate-Like Ni/C as Efficient Bifunctional Electrocatalyst for Hydrogen Evolution and Urea Oxidation, *ACS Appl Mater*

Interfaces, **2018**, *10*, 4750-4756.

[41] R.K. Singh, A. Schechter, Electrochemical investigation of urea oxidation reaction on  $\beta$  Ni(OH)<sub>2</sub> and Ni/Ni(OH)<sub>2</sub>, *Electrochim. Acta*, **2018**, *278*, 405-411.

[42] L. Wang, T. Du, J. Cheng, X. Xie, B. Yang, M. Li, Enhanced activity of urea electrooxidation on nickel catalysts supported on tungsten carbides/carbon nanotubes, *J. Power Sources*, **2015**, *280*, 550-554.

[43] R.K. Singh, P. Subramanian, A. Schechter, Enhanced Urea Activity of Oxidation on Nickel-Deposited Tin Dendrites, *ChemElectroChem*, **2017**, *4*, 1037-1043.

[44] D.D. Zhu, C.X. Guo, J.L. Liu, L. Wang, Y. Dub, S.Z. Qiao, Two-dimensional metal-organic frameworks with high oxidation states for efficient electrocatalytic urea oxidation, *Chem Commun*, **2017**, *53*, 10906-10909.

[45] R.M.A. Hameed, S.S. Medany, NiO nanoparticles on graphene nanosheets at different calcination temperatures as effective electrocatalysts for urea electro-oxidation in alkaline medium, *J Colloid Interf Sci*, **2017**, *508*, 291-302.